

# CIVA CT, an advanced simulation platform for NDT

Marius Costin<sup>1</sup>, David Tisseur<sup>1</sup>, Caroline Vienne<sup>1</sup>, Ronan Guillamet<sup>1</sup>, Hussein Banjak<sup>1</sup>, Navnina Bhatia<sup>1</sup> and Roman Fernandez<sup>2</sup>

<sup>1</sup>CEA, LIST, DISC, 91191 Gif-sur-Yvette, France, e-mail: marius.costin@cea.fr

<sup>2</sup>EXTENDE, Le Bergson, 15 Avenue Emile Baudot, 91300 Massy, France

## Abstract

CIVA CT is a simulation tool for a realistic modeling of the X-ray image formation including photon attenuation and scattering processes and the modeling of various X-ray sources and detectors. Based on a radiographic module, which is the core of the simulation, we are able to create typical CT configurations with the source and the detector moving around a sample. The projection data set obtained with such a configuration can be then used to reconstruct a 3D image with different types of algorithms, implemented as plugins. Moreover, CIVA CT offers the possibility to import real data that can be further processed and reconstructed in the software environment.

**Keywords:** X-ray CT, simulation, CT reconstruction

## 1 Introduction

CIVA is a software simulation platform [1], initially developed for non-destructive testing (NDT) with ultrasound and Eddy currents techniques. Radiographic simulation functionality has been thereafter included and is now completed by the CIVA CT module allowing the simulation of various tomographic configurations. Numerous developments are constantly integrated in this module in order to achieve the final objective of producing a complete chain for NDT inspection with X-ray CT.

In this paper we present an overview of the possibilities offered by CIVA software for X-ray computed tomography simulation. The CIVA CT module models the full physics of photon-matter interaction in a large energy range (from 10 keV to 10 MeV) and is capable of simulating the projection data corresponding to a specific CT scene defined by the user. A multitude of parameters and geometric configurations are available for a maximum versatility of the simulation and for the realization of parametric studies. The software also includes several reconstruction algorithms implemented as plug-ins and dedicated to different acquisition trajectories. These algorithms can be applied to simulated images but also to real ones, which can be loaded into CIVA environment using import functionality and processed with dedicated tools such as the scattering correction.

## 2 Radiographic and CT simulation

### 2.1 Physics model

The simulation code models the physics of photon-matter interaction through the three most important processes in the keV to MeV range: photoelectric effect, Compton scattering and pair production. A fast computation of the attenuation is performed with the Beer-Lambert law, to which a Monte Carlo computation is combined in order to estimate the scattering phenomena. Distinct images are computed and combined into a final one that includes the influence of the X-ray source (size, spectrum and filtering), the attenuation and scattering, the photonic noise and the detector response. Several validation studies have been performed with both experimental data and simulated data generated with other tools to validate the models implemented in CIVA RT/CT.

### 2.1 CT scene

The imaged objects are specified as simple parametric geometrical forms or as complex forms through CAD formats such as stl, step or igs. Flaws can be included and positioned inside the main object and all the objects can be specified as different materials.

The sample, the X-ray source, the detector, the trajectory and the simulation parameters are all defined in a CT scene. Initially only the circular trajectory was handled, but recent developments allow other acquisition geometries, such as helical or partially helical trajectories. Moreover, the trajectory can be specified by a set of points, theoretically enabling any possible choice. Figure 1 presents a 3D view of the simulated configuration with a helical path and a projection without and with noise.

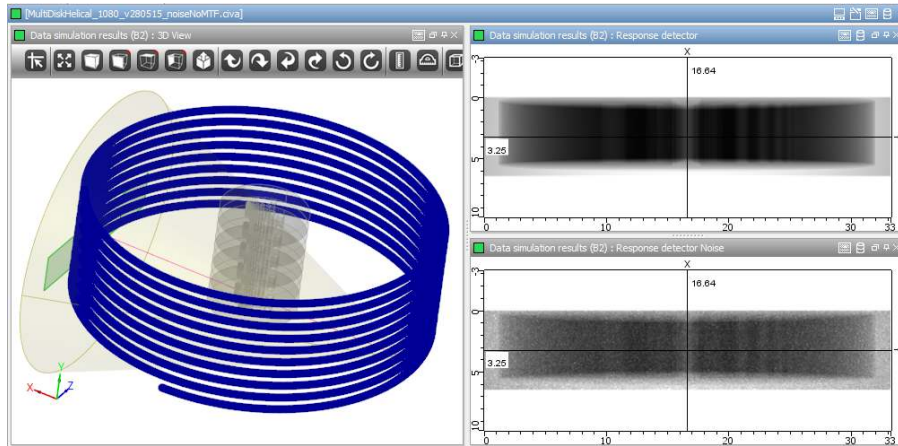


Figure 1: CIVA CT scene and projection data.

### 3 CT reconstruction

Several reconstruction algorithms are implemented as plug-ins to be used on any available data set. These algorithms can handle several acquisition geometries from the classical circular trajectory to more complex ones to deal with long objects and with angular truncation.

#### 3.1 Reconstruction on circular trajectory

Two types of reconstruction algorithms have been implemented in CIVA platform: analytic and iterative. The first one includes the standard Feldkamp-Davis-Kress (FDK) algorithm [2], which is particularly efficient in case of low noise and dense sampling of projections. Recent improvements include an implementation on nVidia CUDA GPU architecture. An adaptive splitting of the reconstruction volume has been developed to allow reconstruction of large volumes. Therefore memory limitations on GPU cards can be overcome. This implementation of FDK algorithm also supports short-scan reconstruction [3].

In the class of iterative methods, two algorithms are well adapted for reconstructions from a small number of projections, namely PixTV [4] and BlobTV [5]. The first uses a pixel-driven projector and a ray-driven back-projector and includes a regularization step with a total variation (TV) norm. The second one uses an irregular grid to describe the imaged object and employs adapted forward- and back-projection operators. An adapted TV regularization is also applied. These two algorithms are implemented only in 2D because of their high complexity. Nevertheless, for small divergence configurations we can safely make the assumption of a multi-fanbeam geometry and we can use them for 3D reconstructions.

Finally, more standard 3D iterative algorithms were developed, using a pixel-driven projector and a ray-driven back-projector with GPU implementation. The same adaptive splitting of the volume as for FDK has been used to avoid GPU memory limitations. Currently, OS-SART algorithm has been implemented and two deriving algorithms: SART, by taking the same number of subset as the number of projections, and SIRT, by taking only one subset containing the entire set of projections. The actual limitation of our 3D algorithm is the size of the RAM of the computer, which must contain simultaneously the set of projections and the reconstruction volume for analytic method and the double for iterative methods.

#### 3.2 Reconstruction on helical trajectories

The circular trajectory for data acquisition is simple and denotes an exact reconstruction only in the central plane of the object. However, when inspecting a long object, this geometry of acquisition creates severe artifacts in the reconstructed image. The multi-disk phantom illustrated in figure 2 is a test object that demonstrates the limitations of the circular trajectory where we can see in Figure 2 (a) the artifacts obtained in the central vertical slice of the 3D reconstructed image. To deal with this aspect known as the long-object problem, the helical scanning geometry was proposed. In 1993, Wang et al. [6] have extended the FDK algorithm to helical trajectory. Figure 2 (b) shows the FDK reconstruction of the multi-disk phantom using a helical scanning geometry.

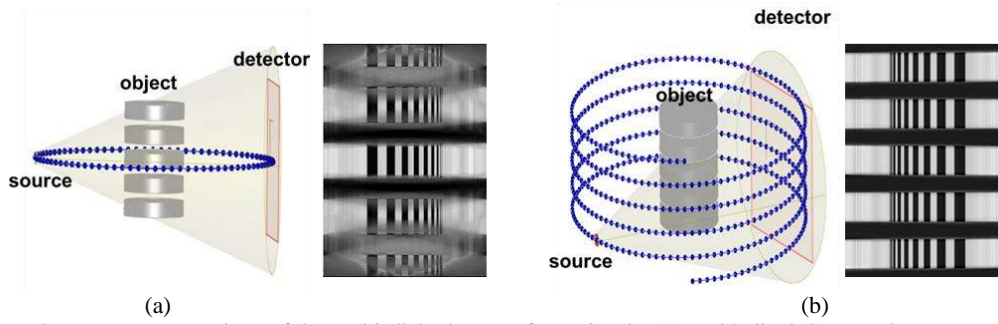


Figure 2: FDK reconstructions of the multi-disk phantom from circular (a) and helical (b) scanning geometries.

In the algorithm we have implemented in CIVa, we have also improved the original version of FDK algorithm to increase its robustness in case of truncated data by modifying the filtering part [7]. Thus the algorithm available in CIVa CT handles region of interest (ROI) reconstruction and avoid the cup artifact usually observed with truncated projections (see Figure 3).

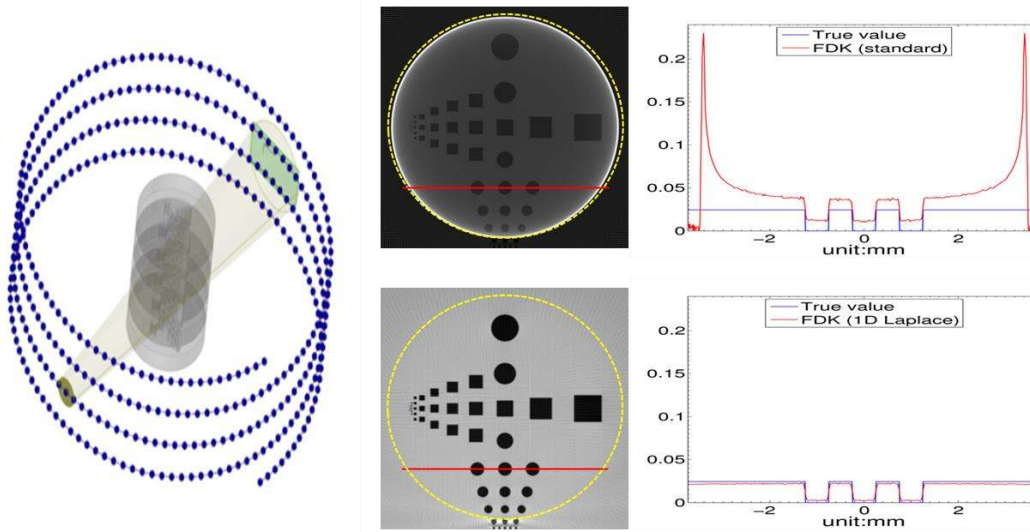


Figure 3: ROI reconstruction in case of truncated data using classical implementation of FDK algorithm (top) and the one we propose (bottom). Corresponding profiles plotted along the red lines show that the cup artefact usually observed (FDK – standard) is avoided with the new filtering we implemented (FDK – 1D Laplace).

### 3.3 Half-scan helical reconstruction

Recently, an FDK-type algorithm for reverse helical trajectory named Fusion-RFDK [8] has been developed which reconstructs the function  $f$  identifying the object from its cone-beam projections  $g$ . The structure of this algorithm consists of the following steps:

(a) Cosine and Parker weighting:  $g'(u_d, v_d, \lambda) = \frac{D}{\sqrt{D^2 + u_d^2 + v_d^2}} w_P(u_d, \lambda) g(u_d, v_d, \lambda)$

(b) Ramp-row-wise filtering:  $g_F(u_d, v_d, \lambda) = \int_{-\infty}^{+\infty} h_r(u_d - u'_d) g'(u'_d, v_d, \lambda) du'_d$ .

(c) Back-projection:  $f^+(\vec{r}) = \int_0^{\lambda_m} \frac{RD}{|R - \vec{r} \cdot \vec{e}_w(\lambda)|^2} g_F(u_d, v_d, \lambda) d\lambda$

$$f^-(\vec{r}) = \int_{-\lambda_m}^0 \frac{RD}{|R - \vec{r} \cdot \vec{e}_w(\lambda)|^2} g_F(u_d, v_d, \lambda) d\lambda.$$

(d) Fusion:  $f(\vec{r}) = f^+(\vec{r}) w_F^+(z) + f^-(\vec{r}) w_F^-(z)$ .

In these equations,  $R$  defines the helical radius,  $D$  refers to the distance source-detector,  $h_r$  is the ramp kernel and  $\vec{e}_w$  is a unit vector oriented from the source towards the center of the detector. The Parker weighting function  $w_P(u_d, \lambda)$  is used to handle redundant data in case of half-scan geometry [9], where half-scan geometry corresponds to a scan over  $180^\circ$  plus the opening angle of the X-ray beam.

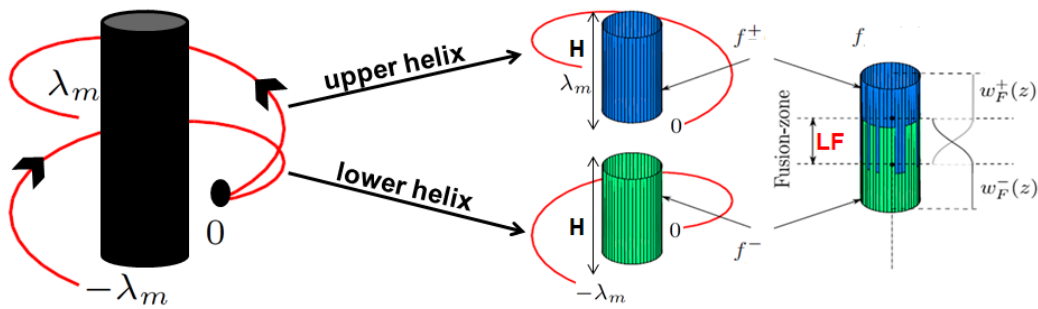


Figure 4: Illustration of the reverse helical geometry and the fusion process in the Fusion-RFDK algorithm [8].

To explain the fusion process, we take two helical turns defined by the endpoints  $-\lambda_m$  and  $\lambda_m$  as illustrated in Figure 4. Using data from these lower and upper helices, respectively, we can reconstruct two functions and merge them using two weighting functions  $W_F^-(z)$  and  $W_F^+(z)$  to obtain the function  $f$  of the object. In equation (d),  $z$  is the axial position of  $\vec{r}$  and  $L_F$  is the length of the zone within which fusion is performed.

We have implemented this algorithm and we show in Figure 5 the reconstruction results using data generated by CIVA. The acquisition geometry and a central horizontal slice of the reconstructed multi-disk phantom are shown in Figure 5(a) and Figure 5(b) respectively. In this simulation, we generate 180 projections over 5 helical turns using a detector of  $256 \times 256$  pixels to reconstruct an image of  $600^3$  voxels. As we can see, these reconstruction results are of good quality.

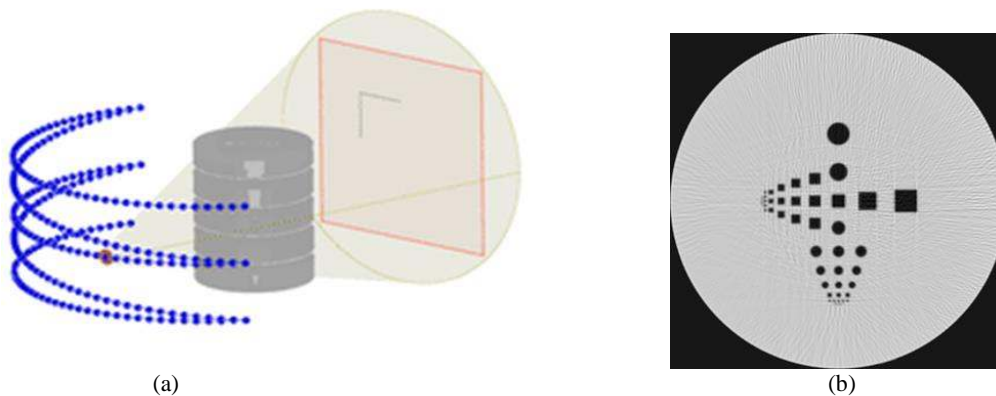


Figure 5: Fusion-RFDK reconstruction of the multi-disk phantom using half-scan reverse helical trajectory.

## 4 Experimental data import and processing

In addition to the simulation of CT configurations, the CIVA CT module also handles experimental data. These data sets can be imported in the software environment to be reconstructed with the various algorithms we have presented in the previous section. Moreover additional post-processing tools, such as scattering correction, are currently being developed to enhance the reconstruction quality.

### 4.1 Experimental data reconstruction

We present results obtained on experimental data sets issued from laboratory CT setups used for various studies. A first data set corresponds to a car engine piston of 82 mm length with a diameter of 78 mm. The sample was scanned with a laboratory CT system using a 225 kV X-ray generator and a flat panel detector in  $2 \times 2$  binning mode. The pixel size is of  $400 \mu\text{m}$  and the image resolution is  $1024^2$  pixels. For this acquisition an angular step of  $0.8^\circ$  was chosen and the distances source-object and object-detector were respectively 827 mm and 236 mm. This data set was loaded in CIVA CT module and the FDK algorithm for circular trajectory was applied to reconstruct the 3D image displayed in Figure 6.

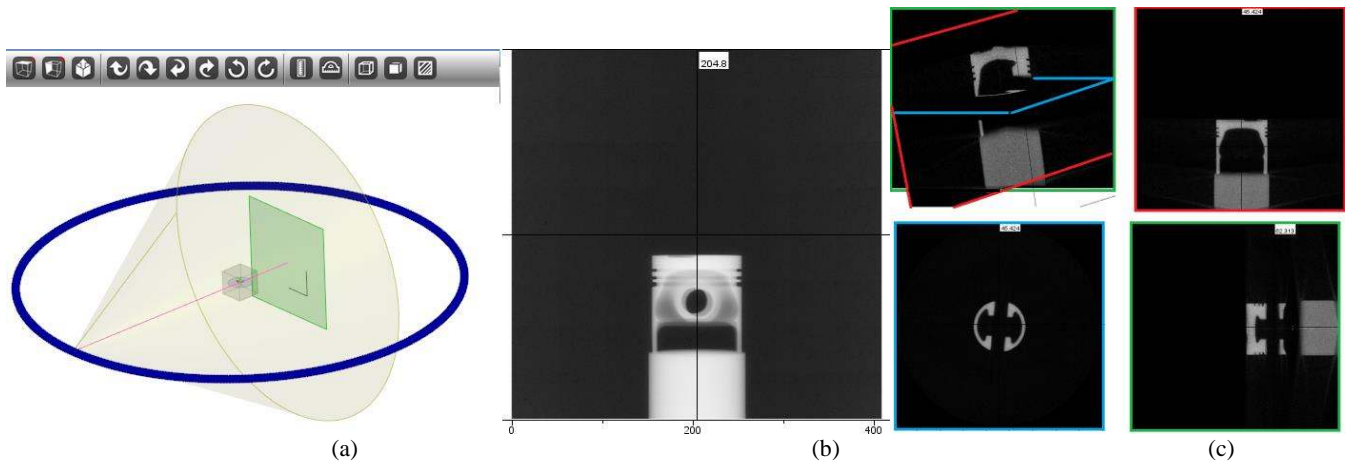


Figure 6: CT of a piston: a) CIVA model of the acquisition geometry, b) real projection image imported in CIVA, c) reconstructed volume with three orthogonal projections.

A second data set comes from a concrete sample scanned on a standard circular trajectory. A cylindrical sample was extracted from a concrete bloc containing metallic reinforcing bars. The sample was scanned with a laboratory CT system composed of a 450 kV X-ray generator and a flat panel detector of 2048x2048 pixels of 200  $\mu\text{m}$ . The acquisition was performed at 200 kV and 3,2 mA. The projection data was imported in CIVA CT and reconstructed with the FDK algorithm. Figure 7 presents the experimental setup, a screenshot with the imported data and the reconstructed volume. Corrections for misalignments were applied, but important metal artifacts are still visible near the reinforcing bars.

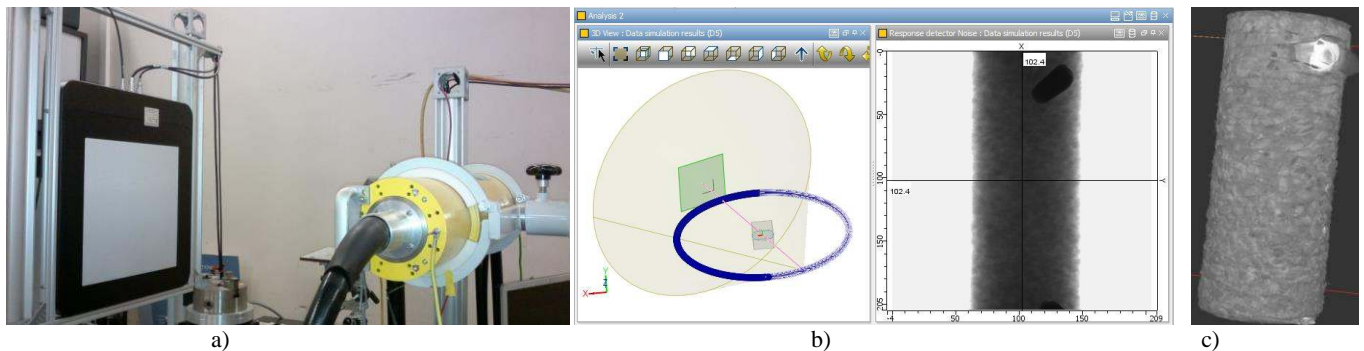


Figure 7: CT of a concrete sample: a) experimental setup, b) data imported by CIVA CT and c) reconstructed volume.

## 4.2 Scattering corrections

Quantitative reconstruction values in CBCT are often miscalculated due to the presence of secondary radiation originating from scattering of photons inside the object and detector under consideration. The effect becomes more prominent and challenging in case of hard X-ray sources (few hundreds of keV) which are very often used in industrial non-destructive testing applications.

We have developed a scatter correction method based on the SKS deconvolution approach proposed by Sun and Star-Lack [10]. Our algorithm is based on a continuous description of the kernel along the traversed thicknesses [11] where the kernels are simulated by means of CIVA software. Figure 8 presents the geometric setup and results for kernels simulation for 400 keV X-ray photons.

We have applied our scatter correction method on an iron hub of height 32 mm and external diameter 52 mm. An X-ray source set at 400 kV was used with 4 mm of Pb and 1 mm of Cd as filtering. The detector used was the Thales Flashscan 33 model [12]. The corrected projections are reconstructed using FDK algorithm in CIVA.

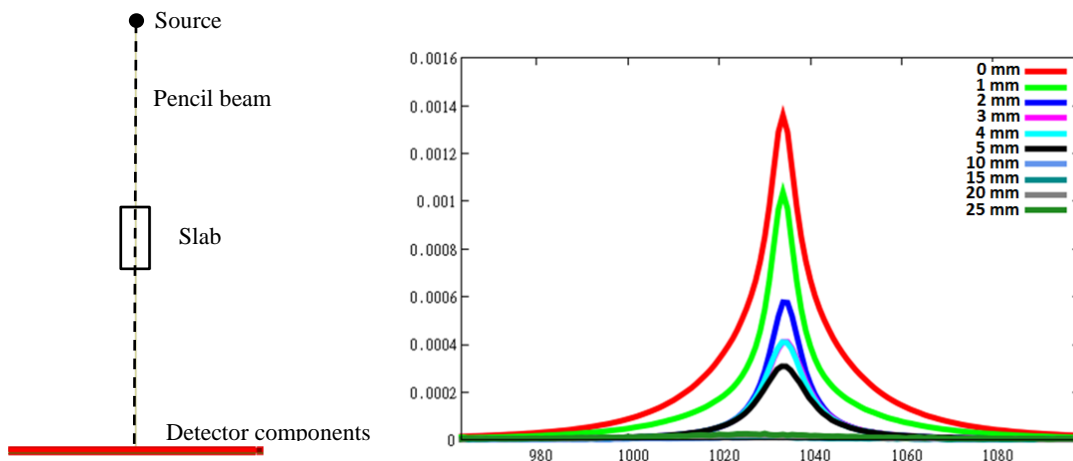


Figure 8: On the left, geometric setup for kernel simulation. On the right side, we display the kernels simulated with CIVA for different iron slab thickness with 400 keV X-ray photon [11].

Figure 9 displays reconstruction slices of the top tip of the iron hub obtained for uncorrected and corrected projections using continuous and discrete methods. Continuous method shows a better edge enhancement compared to the discrete approach in the top tip reconstruction slice as can be seen in Figure 10 and it presents improved reconstruction values as can be seen on the profile plotted along the pink line in Figure 10 (continuous corrected).

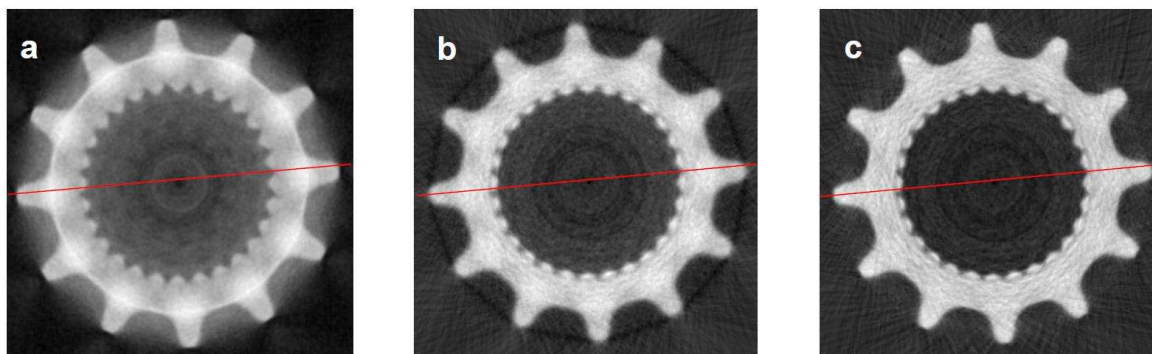


Figure 9: Reconstruction slice of a) uncorrected projections b) corrected projections by discrete method c) corrected projections by continuous method [11].

In the considered energy range the value of the linear attenuation coefficient per cm for a mean energy of 320 keV is 0.83, which is in agreement with the obtained result (see Figure 10). The obtained result of the scatter profile and reconstruction values are also in good agreement with correction performed using beam stop arrays method by A. Peterzol [12], which requires many acquisitions for the correction leading to higher dose.

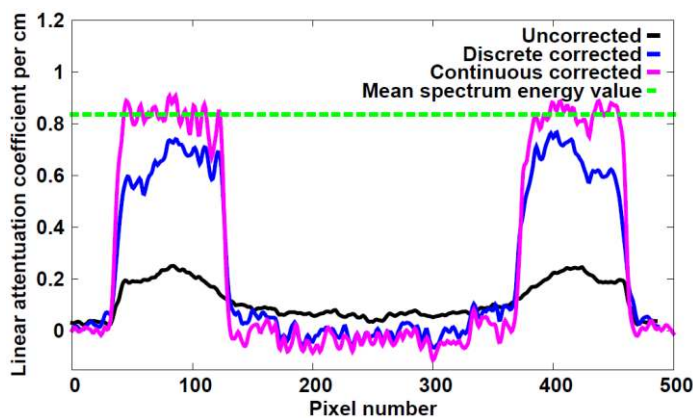


Figure 10: Profile plot of the reconstruction slice of a) uncorrected projections b) corrected projections by discrete method c) corrected projections by continuous method [11].

## 4 Conclusions

CIVA CT is an advanced simulation platform providing a realistic model for radiographic acquisitions in the field of NDT and is capable of simulating the projection data corresponding to a specific CT scene defined by the user. Recent developments include the simulation of complex acquisition trajectories and the implementation of analytic and iterative reconstruction algorithms for circular, helical and semi-helical trajectories. This variety of reconstruction algorithms makes the CIVA CT module fitted to deal with a large range of acquisition configurations, from the standard circular trajectory to more complex ones involving truncation of projection data and limited angular range.

In addition to its simulation capabilities, this module also provides a user-friendly interface for loading and reconstructing experimental data. Coming with this functionality, additional post-processing tools such as scattering correction are currently being developed to further improve the reconstruction quality. As application examples, two experimental data sets were presented on typical NDT samples.

## References

- [1] R. Fernandez, S. Legoupil, M. Costin, D. Tisseur and A. Leveque, "CIVA Computed Tomography Modeling," in 18th World Conference on Nondestructive Testing, Durban, South Africa, 2012.
- [2] L. Feldkamp, L. Davis et J. Kress, «Practical cone-beam algorithm,» *Journal of the Optical Society of America A*, vol. 1, pp. 612-619, 1984.
- [3] Kak et Slaney, *Principles of computerized tomographic imaging*, New York: IEEE Press, 1988.
- [4] H. Wang, L. Desbat et S. Legoupil, «2D X-Ray Tomographic Reconstruction From Few Number of Projections And 3D Perspectives : Applications of Compressed Sensing Theory,» at 10th conference Meeting on fully-3D Image reconstruction in radiology and nuclear medicine, Beijing, China, 2009.
- [5] H. Wang, L. Desbat et S. Legoupil, «Image Representation by Blob and CT reconstruction from Few number of Projections,» chez IEEE MIC, Valencia, Spain, 2011.
- [6] G. Wang, T.-H. Lin, P.-C. Cheng et D. M. Shinozaki, «A general cone-beam reconstruction algorithm,» *IEEE Trans. on Medical Imaging*, pp. 12:486-496, 1993.
- [7] H. Banjak, M. Costin, C. Vienne et V. Kaftandjian, «Two Local FBP Algorithms for Helical Cone-beam Computed Tomography,» chez DIR2015, Ghent, Belgium, 2015.
- [8] Z. Yu, F. Noo, F. Dennerlein, G. Lauritsch et J. Hornegger, «FDK-type Reconstruction Algorithms for the Reverse Helical Trajectory,» chez IEEE MIC, Valencia, Spain, 2011.
- [9] D. Parker, «Optimal short scan convolution reconstruction for fan-beam CT,» *Med. Phys.*, pp. 9:254-257,, 1982.
- [10] M. Sun et J. M. Star-Lack, «Improved scatter correction using adaptive scatter kernel superposition,» *Phys Medical Biol*, pp. 55(22):6675-6720., 2010.
- [11] N. Bhatia, D. Tisseur, F. Buyens et J. M. Létang, «Scattering correction using continuously thickness-Adapted Kernels,» *NDT & E International*, pp. 78:52-60, 2016.
- [12] A. Peterzol, J. M. Letang, D. Babot, «A beam stop based correction procedure for high spatial frequency scatter in industrial cone-beam X-ray CT,» *NIMB*, pp. 266(18):4042-4054, 2008.